A novel microfluidic system for the sensitive and cost-efficient detection of okadaic acid in mussels

Ana Castanheira, Marília Barreiros dos Santos, Laura Rodriguez-Lorenzo, Raquel Queirós, Begoña Espiña*

INL- International Iberian Nanotechnology Laboratory, Avenida Mestre José Veiga s/n 4715-330 Braga, Portugal

12th November 2021
Note added after first publication: This Supplementary Information file replaces that originally published on 9th February 2021.

Supporting Information

A.1. Design and development of the microfluidic chambers

The microfluidic chambers consist of 2 independent pieces of PMMA, delimitated by an O-ring of PDMS (Figure A1. (a)) and supported by screws (Figure A1 (b)). Figure A.1 (c) shows the design of the chamber and its correspondent dimensions (7.5x5x1.5mm).
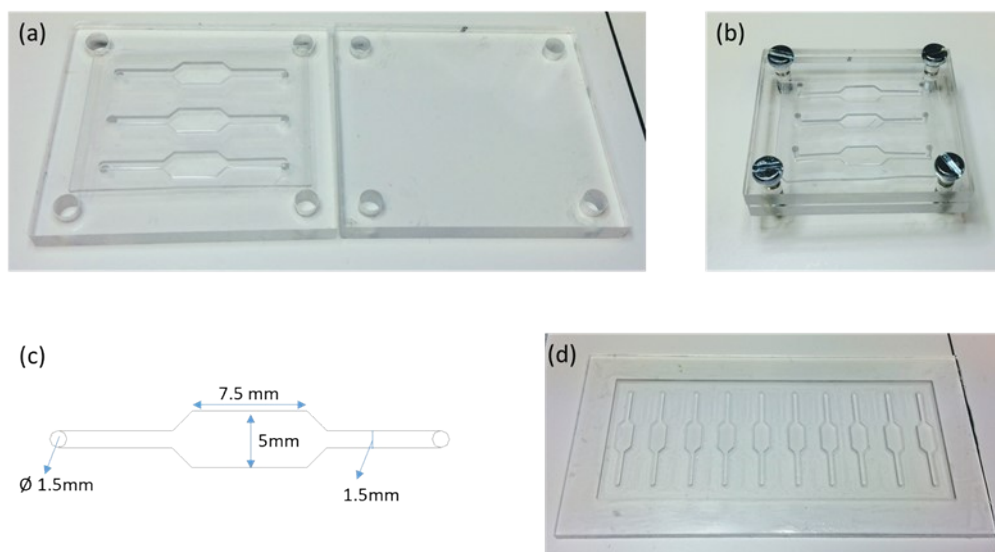

Figure A.1. Image of the (a) disassembled and (b) assembled microfluidic chambers; (c) Design of the microfluidic chambers; (d) mold used for the fabrication of the O-rings.

PDMS O-rings were fabricated by replica molding using a 10:1(w/w) pre-polymer and curing agent mixture. This mixture was poured over the mold (Figure A1. (d)), degassed and cured for 1.5 h at 65 ºC. The two pieces of PMMA and the O-ring mold were designed in ArtCAM and fabricated in PMMA using a Computer Numerical Control (CNC) - High Speed Milling System (FlexiCam Viper, Germany). The top part of the PMMA piece include the inlet and the outlet, which were connected by 1.5 mm O.D. Tygon tube.

A.2. Characterization of sol-gel

A.2.1. Scanning electron microscopy (SEM)

Al_2O_3 sol-gel suspension (50 µL) was deposited on 1×1 cm silicon substrate. After the sol-gel drying overnight at RT, the samples were analyzed by SEM. SEM analysis was

carried out on a FEI Quanta 650 FEG (FEI Europe B.V.) using electron acceleration voltage of 20 (high vacuum mode), at 70 Pa. Secondary electrons were detected by an Everhardt Thornley SED (secondary electron detector).

SEM analysis of the Al_2O_3 sol-gel surface was carried out to compare the surface morphologies. As can be seen in Figure A.2 the surface of Al_2O_3 sol-gel film is a rough surface with globular structures. The rough topography indicates the potential of loading large amount of biomolecules on the surface.
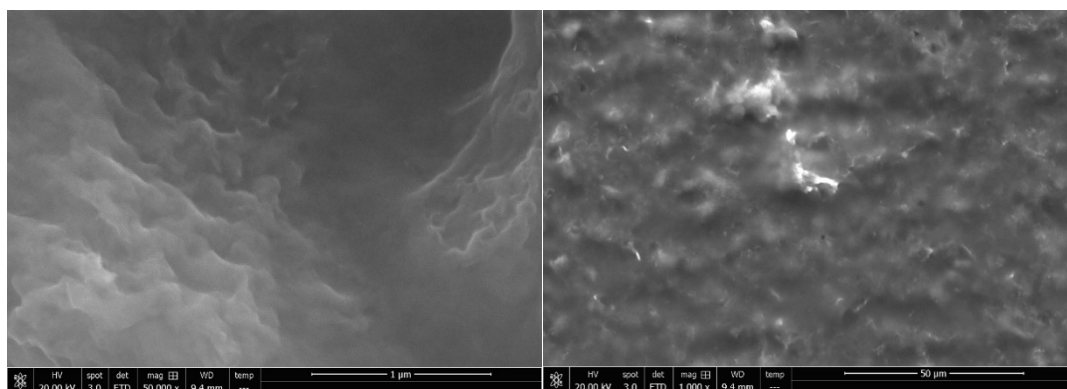

Figure A.2. SEM image of the Al_2O_3 sol-gel surface with magnification of 50000x, Scale bars = 1 µm, (*left*) and 1000x, Scale bars = 50 µm (*right*).

A.2.2. Fourier-transform infrared spectroscopy (FTIR)

The Al_2O_3 sol-gel in PDMS was analyzed using an evacuated optic bench VERTEX 80v vacuum FTIR spectrometer, from Bruker, equipped with a MIR source and a DLaTGs detector operating at RT in spectral range from 12000 to 250 cm^{-1} with KBr window. An ATR (attenuated total reflection) accessory with diamond crystal was used. Data were collected with a 4 cm^{-1} resolution and an accumulated of 64 scans for each spectrum.

Figure A.3. shows the FTIR spectrum of PDMS (blue spectrum) and Al_2O_3 sol-gel on PDMS (yellow). It is possible to see the representative bands of PDMS: Si-O-Si (955 cm^{-1}), Si-CH_3 symmetric rocking (687 cm^{-1}), CH_3 asymmetric rocking + Si-C asymmetric stretching (787 cm^{-1}), CH_3 symmetric rocking (862 cm^{-1}), CH_3 symmetric bending (1262 cm^{-1}), and CH stretching in CH_3 (2950 cm^{-1}).[1] The Al_2O_3 sol-gel spectra presents representative bands at 600 cm^{-1}, 730 cm^{-1} and 1060 cm^{-1}. The band at 1060 cm^{-1} could

3

indicate the vibration modes of Al-O tetrahedra, whereas those around 600 cm^{-1} and 730 cm^{-1} are assigned to stretching vibrations of AlO$_6$ octahedra.[2, 3]
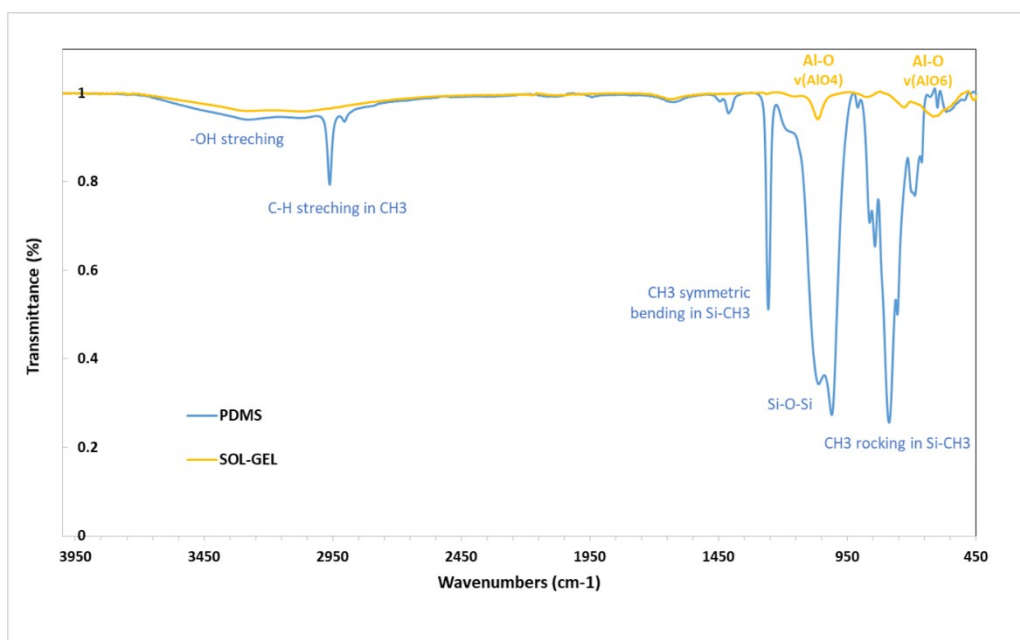

Figure A.3. FTIR spectrum of PDMS (blue spectrum) and Al$_2$O$_3$ sol-gel on PDMS (yellow).

A.2.3. RAMAN

The Al$_2$O$_3$ sol-gel in PDMS was analyzed by Raman spectroscopy (Alpha 300R Confocal Raman microscope Witec) using a 633 nm laser excitation wavelength (grating 600 gr/cm) and a 50 × objective. Acquisition of spectra was performed for 0.5 s and ten scans per measurement were collected at a laser power of 5 mW. The resulting Raman spectra were processed with the Spectragryph software for baseline and cosmic ray removal corrections and Origin 9.0 software for figure preparation.

Figure A.4. shows the Raman spectrum of PDMS (blue spectrum) which has the follow representative bands: Si-O-Si symmetric stretching (488 cm^{-1}), Si-CH$_3$ symmetric rocking (687 cm^{-1}), Si-C symmetric stretching (708 cm^{-1}), CH$_3$ asymmetric rocking + Si-C asymmetric stretching (787 cm^{-1}), CH$_3$ symmetric rocking (862 cm^{-1}), CH$_3$ symmetric bending (1262 cm^{-1}), CH$_3$ asymmetric bending (1412 cm^{-1}).[4] Additionally, the spectrum of the alumina sol-gel produced in the PMMA chamber is also represented. This SERS spectrum clearly shows the vibrational fingerprint of boehmite phase, γ-AlO(OH), which is the predominant phase present the alumina gels formed by hydrolysis/condensation process,[5] dominated by Al-O symmetric stretching mode (357 cm^{-1}), double degenerated

4

mode of the AlO_6 octahedron (498 and 678 cm^{-1}), as described previously.[6] Figure A.3. shows also the Raman spectra of supported on PDMS. As expected, each Raman spectrum resulted in a mixture of the presence of the Al_2O_3 sol-gel and PDMS. However, the characteristic peak centered at 357 cm^{-1} does not overlap with the characteristic peaks of the PDMS.
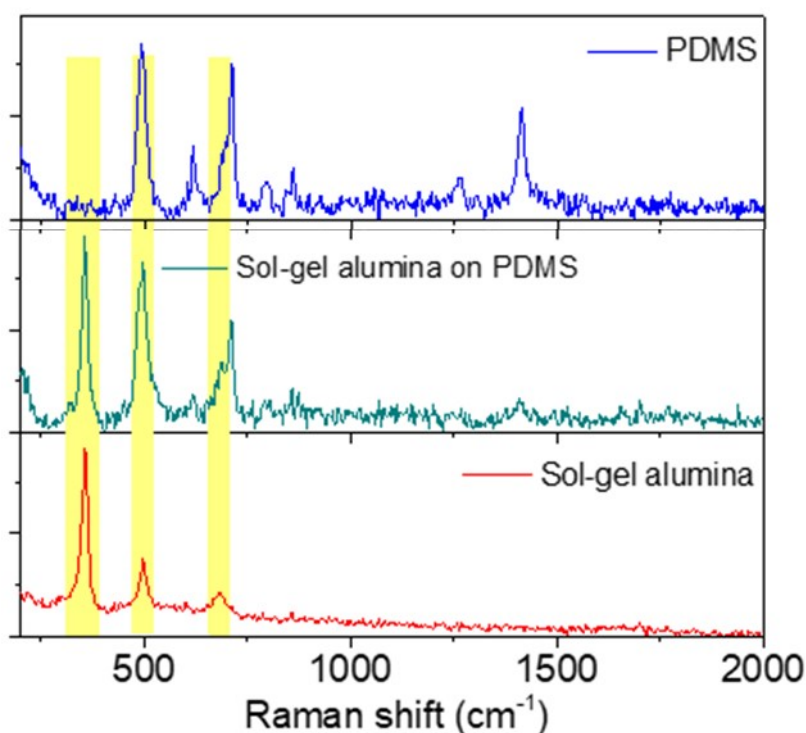
A.4. Raman spectra of PDMS (blue spectrum), alumina sol-gel produced in the PMMA chamber (green) and sol-gel alumina (red). The characteristic peaks for sol-gel are labeled with yellow shaded areas.

A.3. Immobilization of proteins in the microfluidic chamber

The immobilization of proteins in the microfluidic chamber modified with sol-gel was characterized by fluorescence microscopy using fluorescent labelled protein A as standard protein to PP1, since they have a similar molecular weight. A solution of protein A (0.22 mg/mL in PBS) was injected on the sol-gel modified chamber (section 2.4.2), incubated during 1 h and the chambers were finally washed with PBS. The fluorescent images were obtained using a Wide-Field Upright Fluorescence Microscope (Nikon). Figure A.5 shows the results obtained for the immobilized FITC-protein A in sol-gel and its control (without sol-gel). It can be clearly identified the fluorescent signal of the protein

on the sol-gel modified chamber, demonstrating the successful protein immobilization in the Al$_2$O$_3$ sol-gel.
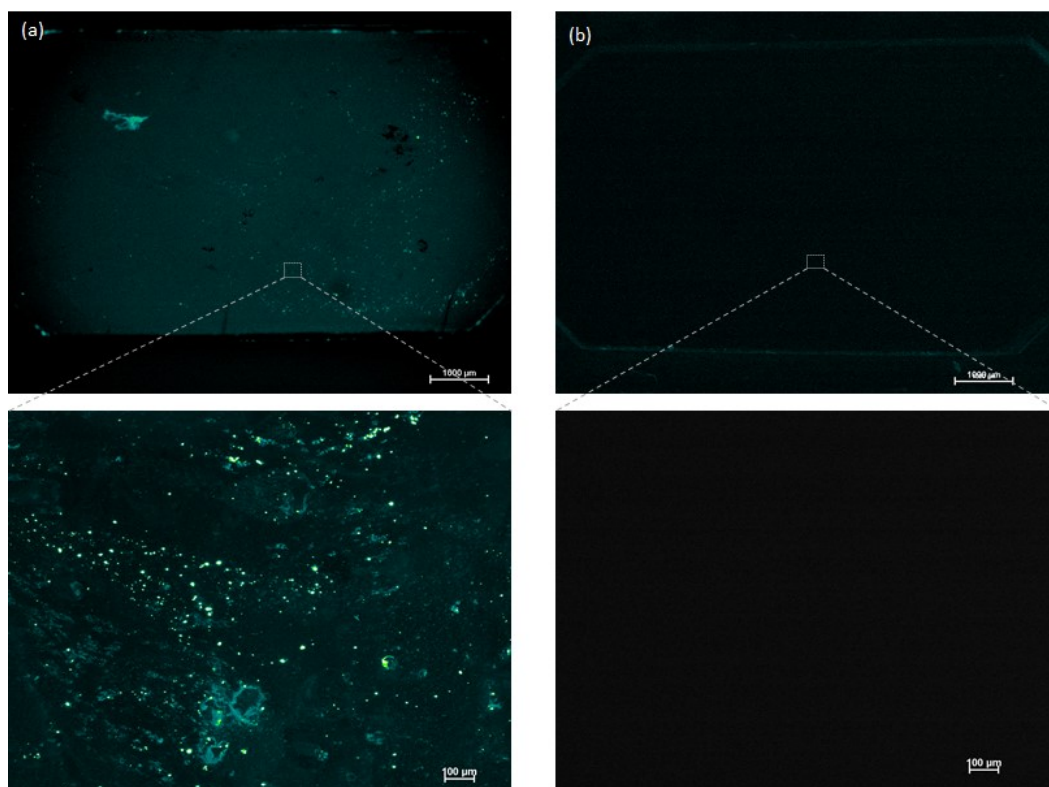

Figure A.5. Fluorescent images for the (a) immobilized FITC-protein A in sol-gel and (b) the control (without sol-gel).

Table A1. Reported sensors platforms for the detection of OA according to the type of sensor,

Author	Detection method	Biorecep tor	Type of sensor	LOD (nM)	Dynamic range (nM)	Reference
Xuan Weng et al 2017	fluorescence	aptamers	PDMS/paper microfluidic aptasensor functionalized by graphene oxide	0.5	0- 7.4	7
Linjiang Panga et al 2019	colorimetric	antibodies	competitive ELISA assay based on epoxy-functionalized magnetic beads	0.4	0.4 – 31	8
Saipriya Ramalingama et al 2019	electrochemical	aptamer	electrochemical microfluidic biochip	0.008	10–250	9
Kaiqi Su et al 2017	image analysis and cell counting assay to monitor the reflection	HepG2 cells	portable smartphone-based cell viability biosensor system	42.7	12.4- 993.7	10
Our work	Colorimetric	PP1	microfluidic system based on PP1 inhibition	11.6 11.0 μg kg^{-1}	43.4 to 3095.8 19.7-15767.3 μg kg^{-1}	

LOD and dynamic range obtained.

References

1. A. R. Passos, S. H. Pulcinelli, V. Briois and C. V. Santilli. (2016) High surface area hierarchical porous Al_2O_3 prepared by the integration of sol–gel transition and phase separation, RSC Adv., 2016,6, 57217-57226.

2. N. P. Damayanti (2010) Preparation of superhydrophobic PET fabric from Al_2O_3–SiO_2 hybrid: geometrical approach to create high contact angle surface from low contact angle materials. Journal of Sol-Gel Science and Technology volume 56, 47–52.

3. Daniela C.L. Vasconcelos Eduardo H.M. Nunes Wander L. Vasconcelos.(2012) AES and FTIR characterization of sol–gel alumina films Journal of Non-Crystalline Solids, 2016, 358, Issue 11, 1374-1379

4. Bae, S. C.; Lee, H.; Lin, Z.; Granick, S. (2005) Chemical Imaging in a Surface Forces Apparatus: Confocal Raman Spectroscopy of Confined Poly(Dimethylsiloxane). Langmuir 2005, 21 (13), 5685–5688.

5. Doss, C.J.; Zallen, R. (1993) Raman studies of sol-gel alumina: Finite-size effects in nanocrystalline AlO(OH). Physical Review B 1993, 48, 15626-15637.

6. Yang, J.; Frost, R.L. (2008) Synthesis and Characterization of Boehmite Nanofibrs. Research Letters in Inorganic Chemistry 2008, 2008, 602198.

7. Weng, X, Neethirajan, S. (2018) Paper-based microfluidic aptasensor for food safety. J Food Saf. 2018; 38:e12412.

8. Linjiang Pang, Haoran Quan, Ying Sun, Pingya Wang, Daifu Ma, Pengqian Mu, Tingting Chai, Yiming Zhang & Bruce D. Hammock (2019) A rapid competitive ELISA assay of Okadaic acid level based on epoxy-functionalized magnetic beads, Food and Agricultural Immunology, 30:1, 1286-1302,

9. Ramalingam S, Chand R, Singh CB, Singh A (2019) Phosphorene-gold nanocomposite based microfluidic aptasensor for the detection of okadaic acid. Biosens Bioelectron 135:14–21.

10. Su K, Pan Y, Wan Z, et al (2017) Smartphone-based portable biosensing system using cell viability biosensor for okadaic acid detection. Sensors Actuators, B Chem 251:134–143.